The effect of structural, electrical &magnetic properties of Ni doped $Sr_{0.98}Zn_{0.02}TiO_3$ ceramics

J.Guravamma & B.H.Rudramadevi*
[1]Research scholar & [2]Assistant professor
Department of physics
Sri Venkateswara University, Tirupati, India

Abstract:

In this paper reports on structural, electrical and magnetic properties of Ni doped $Sr_{0.98}Zn_{0.02}TiO_3$ ceramics prepared by the conventional solid state reaction method. They have been investigated for their structural, morphological, dielectric, electrical and magnetic properties. X-ray diffraction experiment confirms that the cubic structure with Fm3m space group. Field emission scanning electron microscopy (SEM) images illustrated the dense, agglomerated shaped grains. The dielectric and electrical characterization of nickel doped SZT ceramics measurements performed with varying temperature as well as frequency. The dielectric constant and loss are decreases with increasing the frequencies. Frequency dependent of ac conductivity (σ_{ac}) analyses at different temperatures indicate the small polaron hopping frequency. Cole-Cole plots confirm the grain boundary interior, is responsible in the conduction process of the materials. The temperature dependent of zero field cooled (ZFC) and field cooled (FC) magnetization curves demonstrates a ferromagnetic to weak ferromagnetic transition. Improvement in dielectric and magnetic properties makes this material as a promising candidate for multifunctional device applications.

Keywords: $Sr_{0.98}Zn_{0.02}TiO_3$, SEM, XRD analysis, dielectric properties and magnetization

I. Introduction

Alkaline earth titanates, $ATiO_3$ (A = Ca, Sr, and Ba) have been investigated intensively for their advantageous unique dielectric properties, which are of great interest in technological applications such as capacitors, transducers, actuators, and nonvolatile random access memory devices etc. $Sr_{0.98}Zn_{0.02}TiO_3$ is an excellent substrate for epitaxial growth of high temperature super conductors, its mono crystals can be used as optical windows and high-quality sputter deposition targets. SZT based compounds have applications specifically in tunable electronic devices. Strontium zinc titanate is a cubic perovskite material. It is characterized by good mechanical strength, high thermal and chemical stability, low coefficient of thermal expansion, high melting temperature, large nonlinear optical coefficients and, large dielectric constant [1]. By using the strontium zinc titanate for many applications is there. In the manufacture of thermistors [2], multilayer capacitors [3], and electro-optical devices [4], electromechanical devices [5], dynamic random-access memory [6], and field-effect transistors [7]. Superconducting quantum interference device (SQUID) is fabricated using superconductor thin films developed on $SrTiO_3$ substrate [8]. Literature study of transition metal ions doped oxide perovskite materials exhibit the good electrical and magnetic properties. In that reason, I will choose the transition metal ions. Among the all transition metal ions nickel ion is high chemical stability, large magneto crystalline anisotropy and high coercivity. Then I will take the Nickel doped $Sr_{0.98}Zn_{0.02}TiO_3$ ceramics. These ceramics has much potential applications in both magnetic and electrical properties. The dielectric investigation of Nickel doped $Sr_{0.98}Zn_{0.02}TiO_3$ ceramics provide important information on the behavior of localized electric charge carriers, giving rise to a better understanding of the mechanism of dielectric polarization [9]. And the unique magnetic properties of Nickel doped $Sr_{0.98}Zn_{0.02}TiO_3$, depends on the shape, size and purity which are very sensitive to the synthesis method [10]. Until now, different techniques were employed such as the ceramic method [11], co-precipitation [12], the hydrometallurgical processes [13], the sol-gel process [14], complex metric method [15], and microwave [16] etc., for the co-precipitation method, a main challenge is that desired control of particle size is insignificant during synthesize processes [17]. The ceramic method is easy to execute in the industry, but it has high energy consumption. And the hydrometallurgical processes are quite expensive or inefficient in the industry. Among various preparation methods, the solid state reaction method was found to be a suitable method with their simplicity, better control ratio, environment friendly and non toxic [18]. In this present work, here we demonstrated a systematic study on the synthesis of structural, dielectric and magnetic properties of nickel doped $Sr_{0.98}Zn_{0.02}TiO_3$ ceramics by conventional solid state reaction method, and the characterization was consummate using various techniques like XRD, SEM, EDAX, Dielectric measurements, and VSM.

II. Experimental & Characterization Techniques

Ceramic samples of $Sr_{0.98}Zn_{0.02}TiO_3$ and $Sr_{0.98}Zn_{0.02}Ni_xTi_{(1-x)}O_3$ (where x = 0.1, 0.2 and 0.3) were prepared by traditional solid state reaction method. Stoichiometric quantities of high-purity (99.99%) $SrCO_3$, TiO_2, ZnO and NiO_2 powders were taken according to chemical formula and mixed thoroughly using agate mortar for 1 hour. Mixed powders were calcined in air at 1000 °C for 4 h. The calcined powders were added with poly vinyl alcohol (PVA) solution and pressed into disc-shaped pellets. The

obtained pellets were then heat-treated at 900 °C for 2 h to eliminate PVA, and we get the final powder pellets was used for further characterizations. X-ray diffraction pattern was collected using a Philips diffractometer with Cu K_α radiation. The microstructure and morphological studies of the ceramics were observed by using Carl Zeiss field emission scanning electron microscope (FESEM) operated at 20 KV. The dielectric and electrical properties were examined by means of HIOKI 3532-50 LCR Hi TESTER and TEP measurement kit. Magnetic measurements were made by using Lakeshore, USA, Model 7407 Vibrating Sample Magnetometer (VSM) at different temperatures in zero field cooling (ZFC) mode the magnetization curves dependent on temperature, were plotted. For FC measurement, the sample was first cooled down up to room temperature (300 K) and then the data was collected during the warming process in a small field of 500 Oe. All the measurements were performed at different temperatures.

III. Results & discussions

XRD analysis

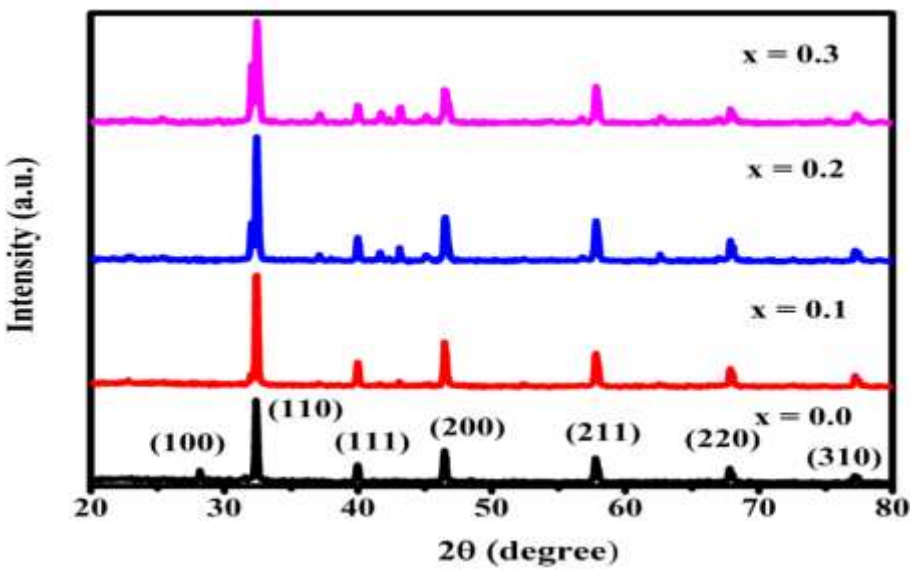

Figure 1. XRD profile of $Sr_{0.98}$ Zn $_{0.02}$ TiO_3 and $Sr_{0.98}$ $Zn_{0.02}$ Ni_x $Ti_{(1-x)}$ O_3 (where x = 0.1, 0.2 and 0.3) ceramics

The prepared samples were analyzed by powder X-ray diffraction using Cu-K_α radiation (λ=1.5406 Å) with 2θ ranging from 20˚ to 80˚ with a scan rate of 0.02 steps per second. Figure1showsthe XRD pattern of the Ni doped $Sr_{0.98}Zn_{0.02}TiO_3$ ceramic powders and they are indexed on the basis of the reflections from the JCPDS file no.84- 0443. The major phase was identified to be cubic with, (110),(111),(200),(210),(211),(220) and (310) reflections appearing at 32.0˚, 39.7˚, 46.1˚, 52.0˚, 57.5˚, 67.6˚, and 77.1˚ 2θ positions respectively. For nickel doped strontium zinc titanate phase transition will be occurred. The symmetries changes from the one crystal system to another one that is cubic to tetragonal or orthorhombic or monoclinic. For cubic → tetragonal system is presented in the $Sr_{0.98}Zn_{0.02}Ni_xTi_{(1-x)}O_3$ powder diffraction. In this system the (100) cubic peak splits in to two peaks with indices 100 and 001 in that case a ≠ c. Likewise the 110 cubic peak will splits in to two peaks with indices 110 and 101.However, the 111 cubic peak will not split under this symmetry transformations. The 200 cubic peak will be split into two peaks with indices 200 and 002.The interplanar spacing for (011); i.e.,d_{110} was calculated from the corresponding 2θ position using Bragg law. It has been found that the crystallite size of samples decreases with Co doping. The decrease in crystallite size is closely associated with the incorporation of Co^{2+} ions inside the $Sr_{0.98}Zn_{0.02}$ Co_x $Ti_{(1-x)}O_3$ matrix, which consists of larger ionic radii as compared to Ti^{4+} ions. The remaining parameters such as dislocation density (ρ) and lattice strain (ε) were listed in table 1.

Table1. The observed crystalline size, strain values and dislocation density values of $Sr_{0.98}Zn_{0.02}Ni_xTi_{(1-x)}$ O_3 ceramics.

Formula $Sr_{0.98}Zn_{0.02}Ni_xTi_{(1-x)}$ O_3	Crystalline size (D) nm	Lattice strain (ε)	Dislocation density (ρ)lines/meter^2
$Sr_{0.98}Zn_{0.02}TiO_3$ (x = 0.0)	45	2.9 x 10^{-3}	4.93 x 10^{-4}
$Sr_{0.98}Zn_{0.02}Ni_{0.1}Ti_{0.9}$ O_3 (x = 0.1)	44	3.0 x 10^{-3}	5.09 x 10^{-4}
$Sr_{0.98}Zn_{0.02}Ni_{0.2}Ti_{0.8}$ O_3 (x = 0.2)	41	3.2 x 10^{-3}	5.8 x 10^{-4}
$Sr_{0.98}Zn_{0.02}Ni_{0.3}Ti_{0.7}$ O_3 (x = 0.3)	42	3.1 x 10^{-3}	5.58 x 10^{-4}

SEM & EDS analysis

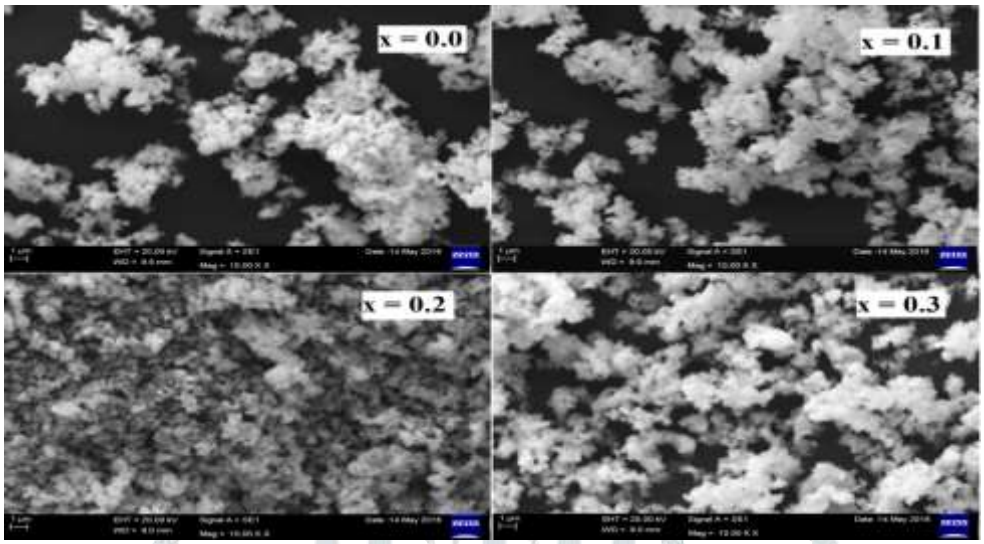

Figure 2(a) SEM image of $Sr_{0.98}$ Zn $_{0.02}$ TiO_3 and $Sr_{0.98}$ $Zn_{0.02}$ Ni_x $Ti_{(1-x)}$ O_3 (where x = 0.1, 0.2 and 0.3) ceramics

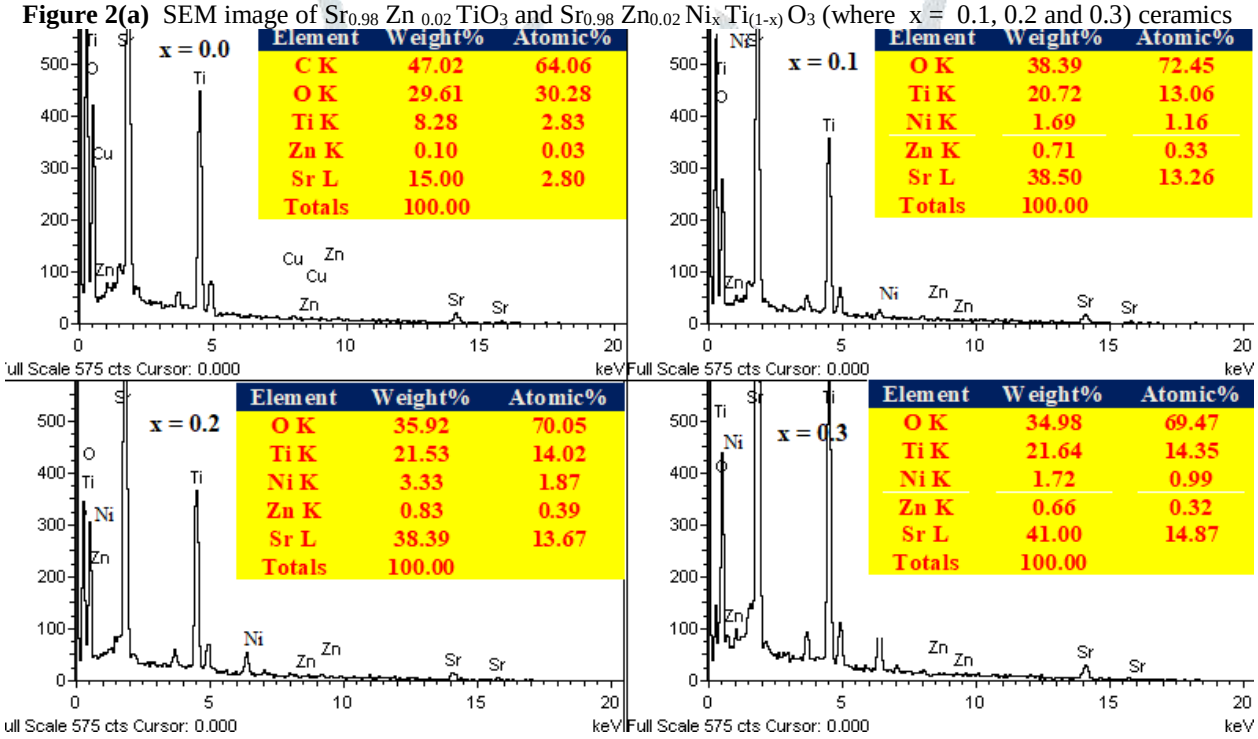

Figure 2(b) The elemental analysis of $Sr_{0.98}$ Zn $_{0.02}$ TiO_3 and $Sr_{0.98}$ $Zn_{0.02}$ Ni_x $Ti_{(1-x)}$ O_3 (where x = 0.1, 0.2 and 0.3) Ceramics

The figures 2(a) & 2(b) shows the surface topography of $Sr_{0.98}Zn_{0.02}TiO_3$ and $Sr_{0.98}$ Zn $_{0.02}$ Ni $_x$Ti $_{(1-x)}$ O_3 (where x= 0.1, 0.2 and 0.3) ceramics respectively, which were analyzed by using the scanning electron microscopy. The micro structural representation of these ceramics was shows regular and spherical grains. The particles are found to be agglomerated on doping with Ni into the matrix of $Sr_{0.98}Zn_{0.02}TiO_3$. Further, the elemental analysis was analyzed by using the energy dispersive X-ray analysis (EDS). The figure shows the appearance of the strontium (Sr), Titanium (Ti), Zinc (Zn), Nickel (Ni) and Oxygen (O) in the lattice of the prepared ceramics. The weight percentage (wt. %) and atomic percentage (at. %) of the constituent elements are tabulated in inset.

Dielectric measurements

Frequency dependence of dielectric constant

In an applied ac field, the complex form of the dielectric constant is $\varepsilon = \varepsilon' + j\varepsilon''$, where ε' denotes the real part of dielectric constant and ε'' harmonize to the imaginary part of dielectric permittivity. The dielectric loss is represented by well-known parameter $\tan\delta = \varepsilon''/\varepsilon'$ where δ denotes the phase difference of applied field to that of induced current. The dielectric constant was calculated using this formula.

$$\varepsilon' = \frac{cd}{\varepsilon_\circ A}$$

Where c is the capacitance, A is the area, d is the thickness of the pellet, ε_o is the permittivity of free space (8.85 x 10^{-12} farad/m).

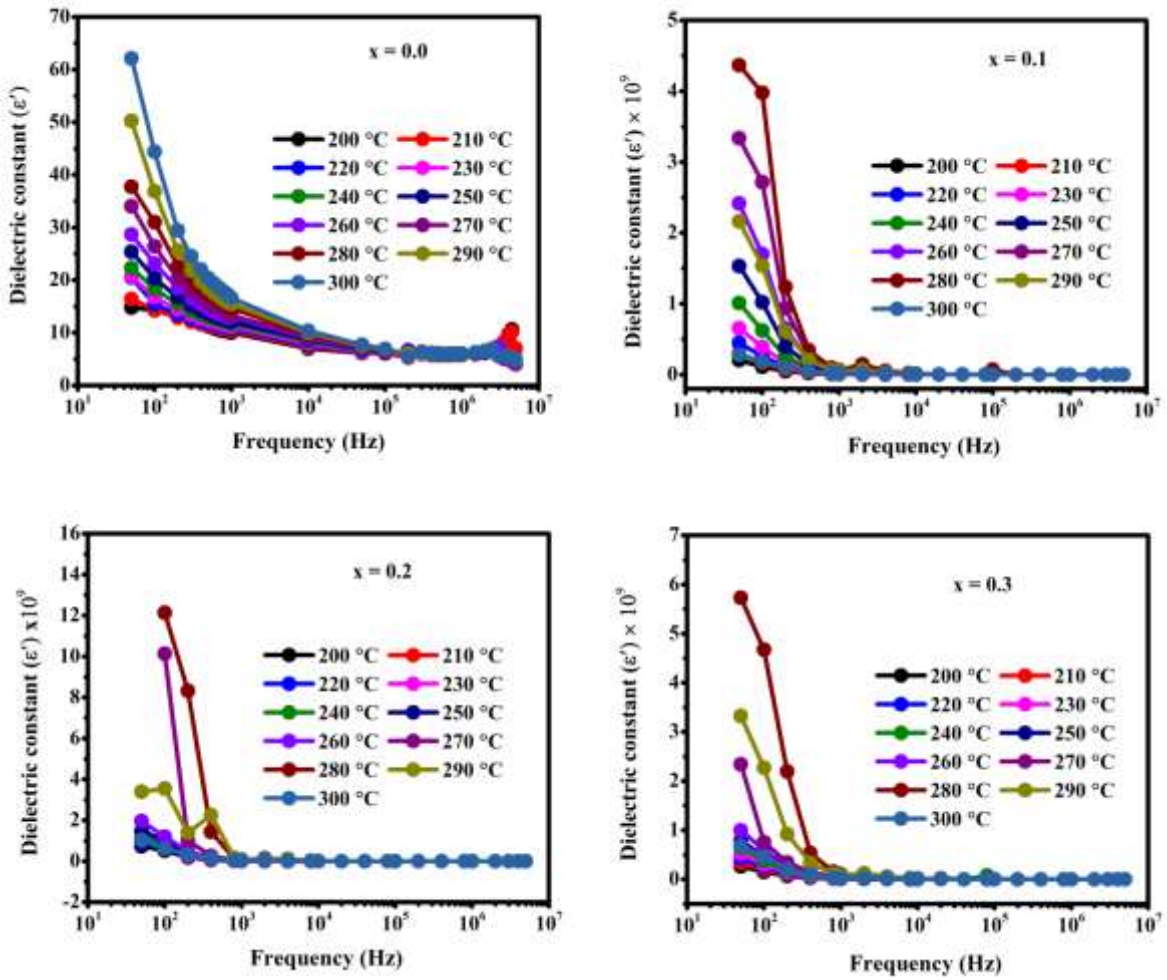

Figure 3. Frequency dependence of dielectric constant (ε′) of $Sr_{0.98}Zn_{0.02}Ni_xTi_{(1-x)}O_3$ (where x = 0.0, 0.1, 0.2 and 0.3) ceramics.

The frequency dependence of the dielectric constant (ε′) for $Sr_{0.98}Zn_{0.02}Ni_xTi_{(1-x)}O_3$ at different temperatures as shown in fig 3. For all the compounds, the dielectric constant is shows a usual decreasing behavior with increasing frequencies. From the figure at lower frequencies, is about (<1 KHz) the dielectric constant is increases, while at higher frequencies (> 1 KHz) it decreases slowly and becomes it is almost frequency independent. At low frequencies, the polarization of ferroelectrics is almost contributed by the polarization of dipoles, this behavior is normal for ferroelectric materials. The high values of ε′ at low frequency region; it may be due to in the presence of all types of polarizations (electronic, ionic and orientational) including space charge, which dominates at low frequency region. The decrease of dielectric constant at high frequency region shows the Maxwell-Wagner interfacial polarization model and is consistent with Koop's theory of dielectrics. According to the Koop's theory of dielectric materials, the dielectric structure is composed of conducting grains and insulating grain boundaries. At lower frequencies, the effect of grain boundaries dominates over grains, because in this reason, at low frequency region, the poorly conductive grain boundaries, due to their interior morphological defects, are more effective while smooth grains which are highly conducting are effective at high frequency [19]. Thus, the decreased behavior of permittivity at high frequency is mainly

attributed to the interior grains as the hopping of the charge carriers do not follow the external field, it is difficult with a small interval of time [20].

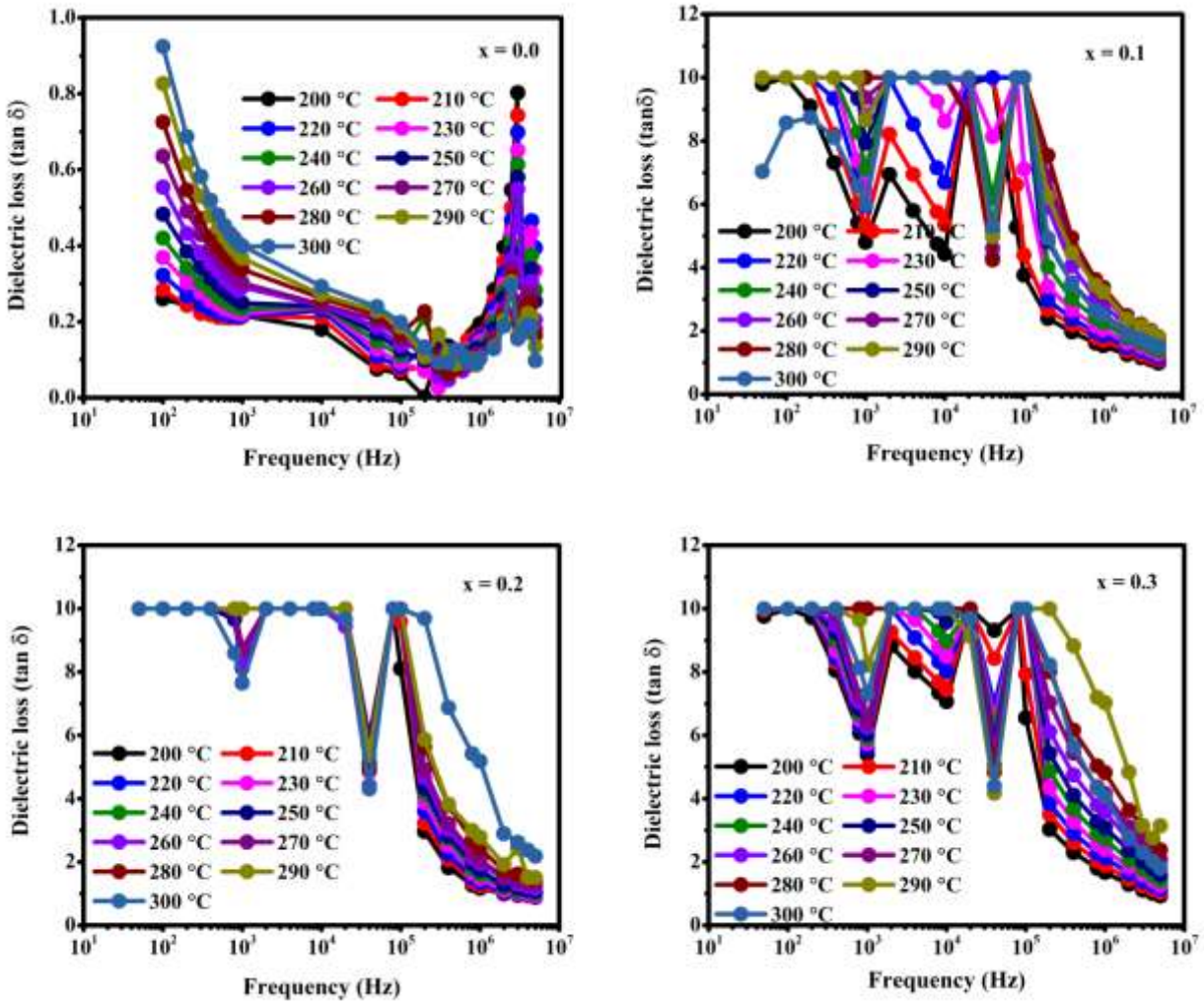

Figure 4. Variation of dielectric loss with frequency at different temperatures of $Sr_{0.98}$ Zn $_{0.02}$ Ni_x $Ti_{(1-x)}$ O_3 (where x = 0.0, 0.1, 0.2 and 0.3) ceramics.

Fig 4 shows dielectric loss factor tan δ of the $Sr_{0.98}$ Zn $_{0.02}$ Ni_x $Ti_{(1-x)}$ O_3 (where x = 0.0, 0.1, 0.2 and 0.3) ceramics as a function of frequency with different temperatures. At low frequency, the dielectric loss is large and decreases rapidly at increase of frequency. The decrease in tan δ with increasing frequency is associated with lagging behind of ions charged species with applied field which contributes towards polarization [21]. However, a reverse trend is obtained for tan δ when the frequency is higher than 10^6 from the host material. The dielectric loss is increased with increasing the temperature. The high frequency, the dielectric loss decreased. Because at that region several parameters influenced on the ceramic materials. These are composition, the purity of starting materials, processing conditions, sintering temperature, and porosity of the materials. Thus for the low values of dielectric loss at higher frequencies, Ni doped $Sr_{0.98}Zn_{0.02}TiO_3$ samples used potential applications in high frequency devices [22].

Ac conductivity analysis

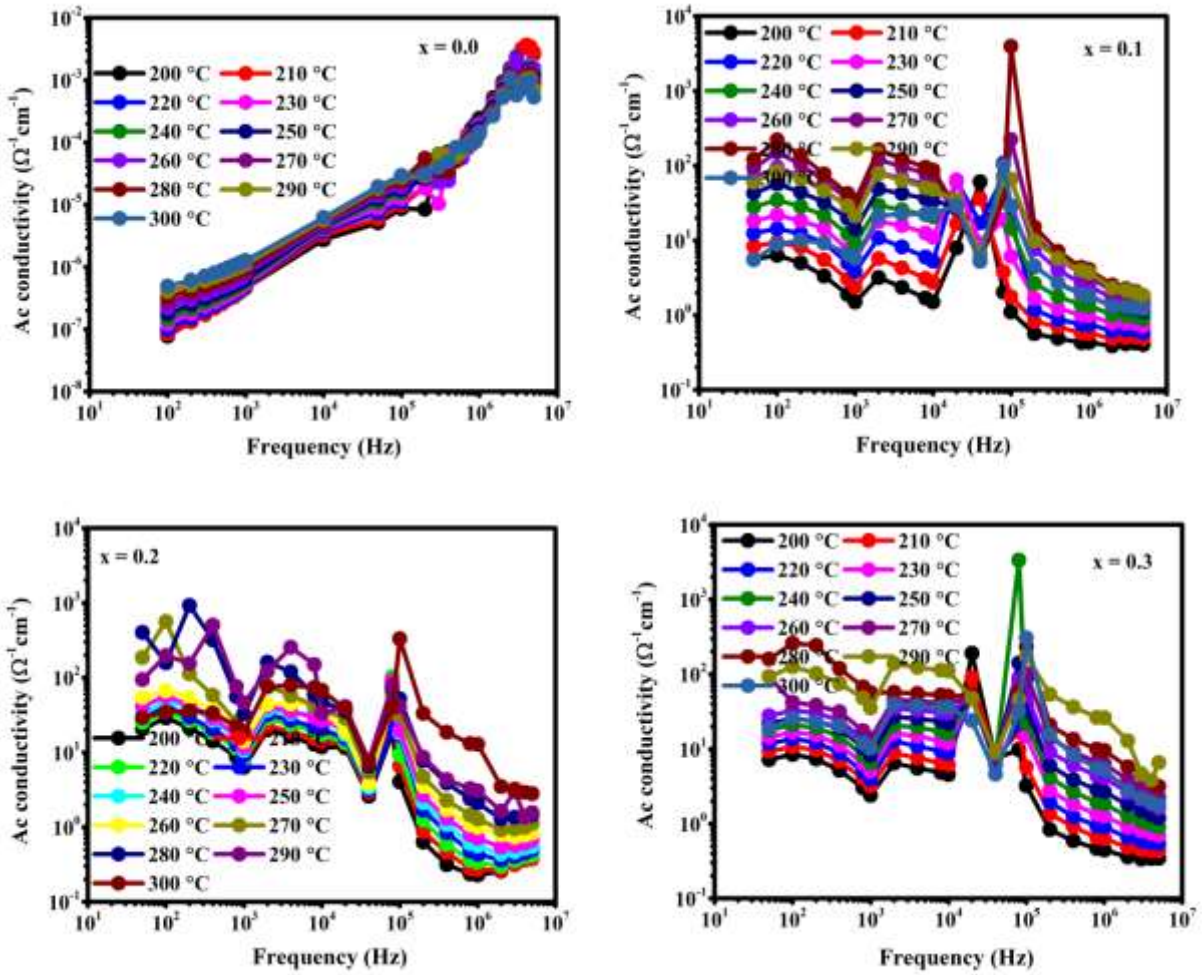

Figure 5. The variation of ac conductivity (σ_{ac}) of $Sr_{0.98}Zn_{0.02}Ni_xTi_{(1-x)}O_3$ (where x = 0.0, 0.1, 0.2 and 0.3) ceramics as a function of frequency with different temperatures.

To study the conductivity of the charge carriers, frequency dependence of ac conductivity is a well traditional method. The plots of frequency dependence of the ac conductivity, at different temperatures for $Sr_{0.98}Zn_{0.02}Ni_xTi_{(1-x)}O_3$ ceramics, as shown in fig 5. The ac conductivity was calculated using this empirical formula [23].

$$\sigma = \omega \varepsilon_{\circ} \varepsilon' \tan \delta$$

Where $\omega = 2\pi f$ is angular frequency and ε_0 is permittivity of free space and has the value 8.852×10^{-12} Fm^{-1}. For all the samples, in this low frequency range up to 10^4 Hz , a frequency independent behavior is observed and at linear increase in conductivity as increasing the temperature because at low frequencies are assigned to the blocking electrode polarizations. At higher frequencies ($>10^4$ Hz), the variation of conductivity becomes less sensitive to temperatures whereas it shows a relatively frequency dependent behavior, this is due to ionic conductivity of the materials at high frequency region [24]. With increase the temperature it is observed that, the σ_{ac} conductivity is increases, and merged at high frequency region, for all selected temperatures. Because in this high frequency region, it increases the drift mobility of the charge carriers of hopping frequency [25]. In general, the behavior of electrical conductivity in solids follows Jonsher's power law [26], given as:

$$\sigma(\omega) = \sigma_{dc} + A\,\omega^s$$

Where, σ (w) is the total conductivity , σ_{dc} is the frequency independent dc conductivity, s and A are the frequency exponent and pre - exponential factors respectively, which are both temperature and material dependent. The term $A\omega^s$ represents the frequency dependence and characterizes all dispersion phenomena. Fig. 5 shows the increase in σ_{ac} for all the samples with increasing the temperature.

Complex impedance spectroscopy study

To understand the conduction mechanism in the Ni doped $Sr_{0.98}Zn_{0.02}TiO_3$ ceramic samples, we have represented the frequency dependence of the real part of impedance (Z') and imaginary part of impedance (Z'') of the complex impedance spectrum, at different temperatures.

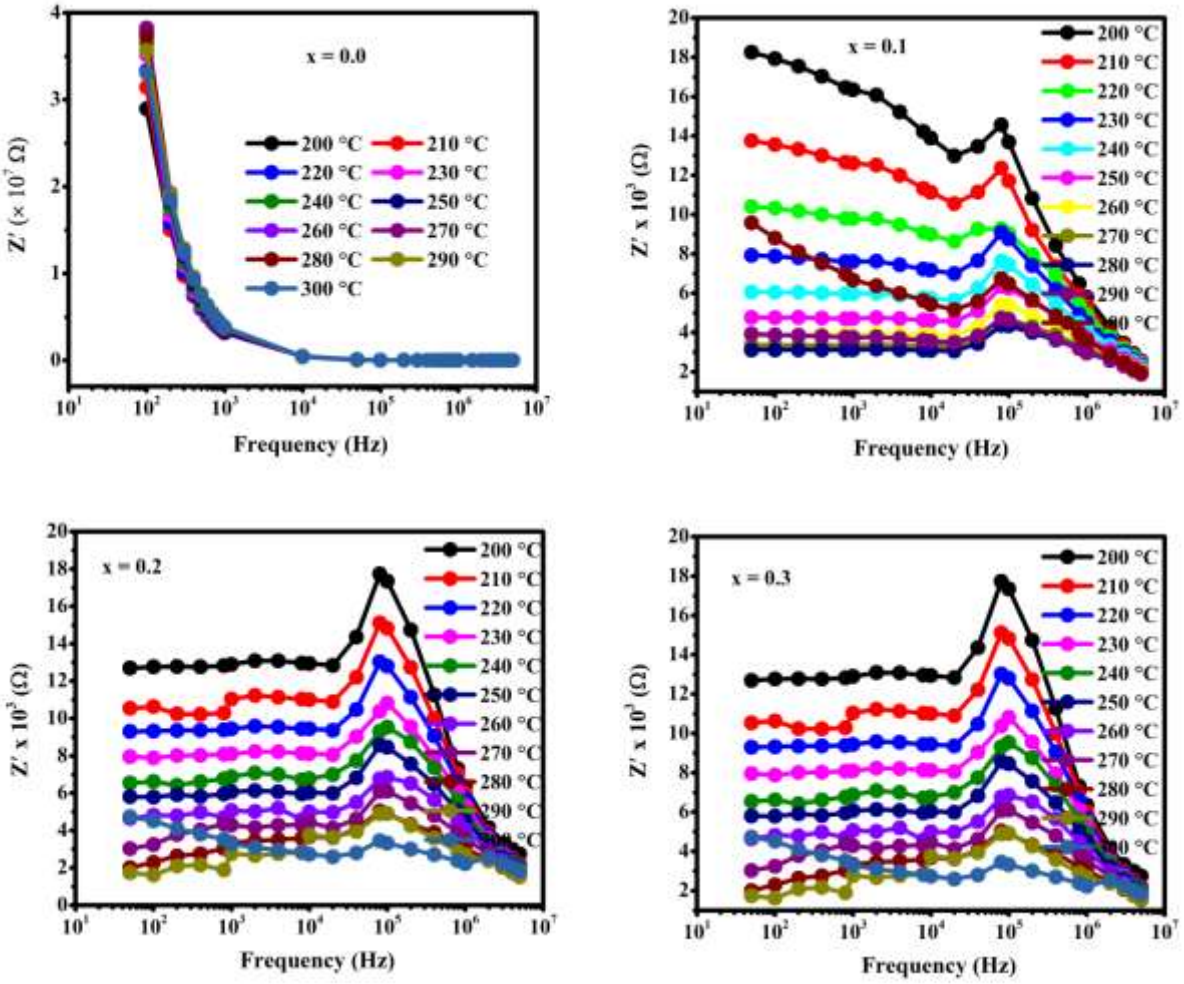

Figure 6 (a). Variation of real part of impedance (Z′) with frequency of $Sr_{0.98}$ Zn $_{0.02}$ Ni $_x$ $Ti_{(1-x)}$ O_3 (where x = 0.0, 0.1, 0.2 and 0.3) ceramics at different temperatures.

Fig. 6 (a) Shows the variation of real part of impedance (Z') with frequency at different temperatures for $Sr_{0.98}Zn_{0.02}$ $Ni_xTi_{(1-x)}$ O_3 ceramic samples. It is observed that $Sr_{0.98}Zn_{0.02}TiO_3$, the Z′ value has higher values at lower frequencies and it decreases progressively with increase in frequency which may due to the ceramic polarization effect. The Ni doped $Sr_{0.98}Zn_{0.02}TiO_3$, the magnitude of Z' is found to decrease with the rise in temperature and their values for all temperatures merge in the higher frequency region. The decrement of Z' with rise in the value of temperature and frequency may be due to increase in ac conductivity with temperature and frequency. It is observed that $Sr_{0.98}Zn_{0.02}TiO_3$ and Ni doped $Sr_{0.98}Zn_{0.02}TiO_3$ the lines are merger for all temperatures in the high frequency region, suggests a possible release of space charge and a consequent lowering of the barrier properties in the materials [27]. It has also been observed that at any particular temperature the impedance value decreases with the increase in doping concentration of Ni^{2+}. To calculate the real part of the impedance by using this formula.

$$Z' = \frac{R}{1 + (\omega RC)^2}$$

Where w is the angular frequency, R is resistance and C is the capacitance of the sample. By using this formula to obtain the electrical processes of the ceramics samples at largest resistance.

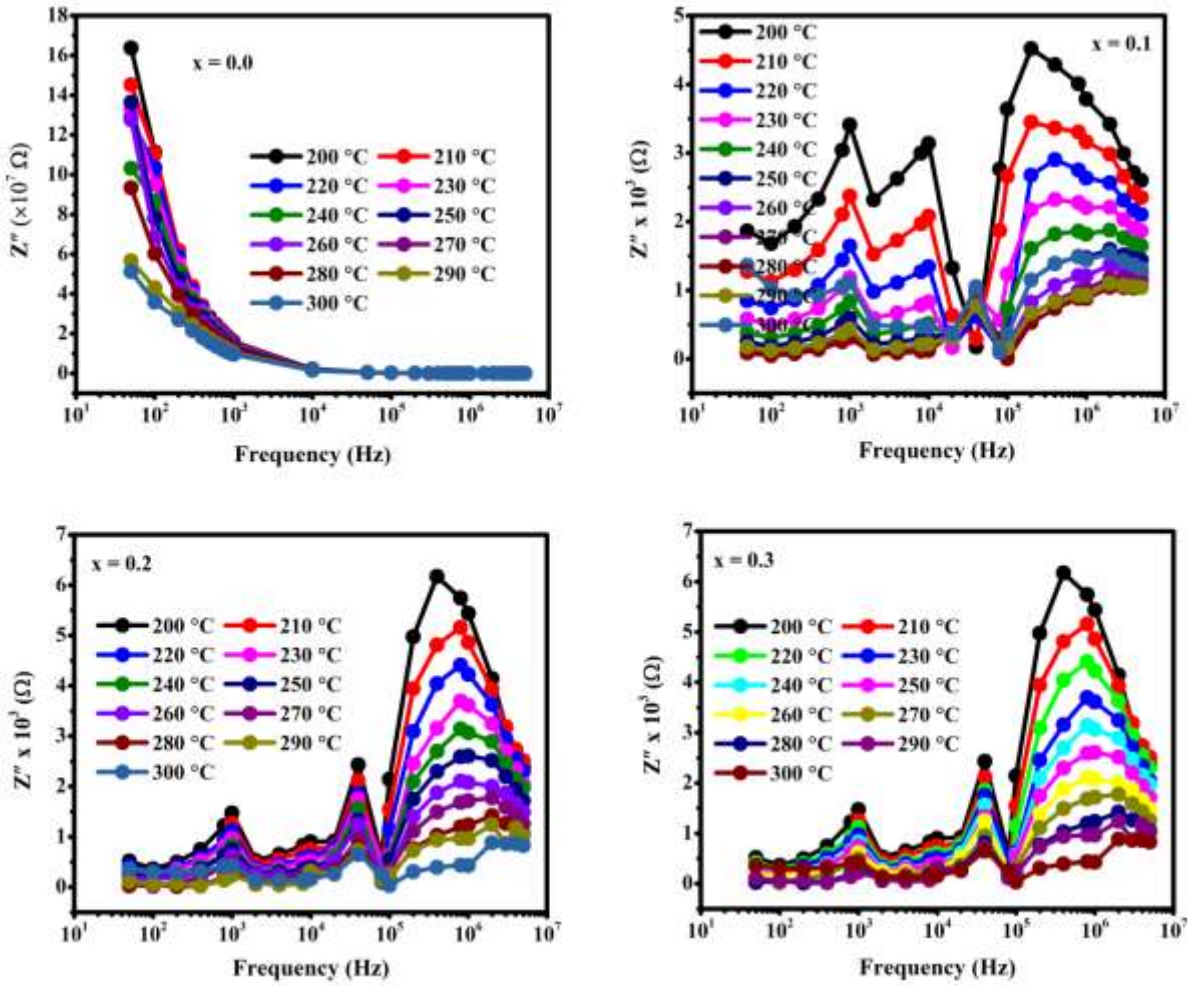

Figure 6 (b). Variation of imaginary part of impedance (Z″) with frequency of $Sr_{0.98}$ $Zn_{0.02}$ Ni $_x$ $Ti_{(1-x)}$ O_3 (where x = 0.0, 0.1, 0.2 and 0.3) ceramics at different temperatures.

Fig. 6(b) Represents the variation of imaginary part of the impedance (Z″) with frequency for $Sr_{0.98}Zn_{0.02}Ni_xTi_{(1-x)}O_3$ ceramics at different temperatures. This imaginary part of the impedance spectrum allows one and to obtain information on the electrical processes having the largest resistance. The largest resistance was calculated using this relation. The following relation is

$$Z'' = \frac{\omega R^2 C}{1 + (\omega RC)^2}$$

Where w is the angular frequency, R and C are resistance and capacitance of the sample. At Ni doped $Sr_{0.98}Zn_{0.02}TiO_3$ ceramics, by the appearance a small peak at a lower frequencies, and increasing the frequency peak height is increases, the asymmetric peak broadening occurs which suggests electric processes in the material with a relaxation time spread as indicated by the peak width. This is due to relaxation process in the material at higher frequency region [28]. With increasing the temperature region, the decrease in the magnitude of the peak, and shift to higher frequency region with an increasing to Ni concentration. They merge in the high-frequency domain which indicates space charge polarization appearance at the lower frequency and its disappearance at a higher frequency [29]. Peaks shifting towards the higher frequency side upon substitution of Ni^{2+} at the Ti^{4+} site which is assumed during the calculation of charge component balancing in $Sr_{0.98}Zn_{0.02}TiO_3$ ceramics systems.

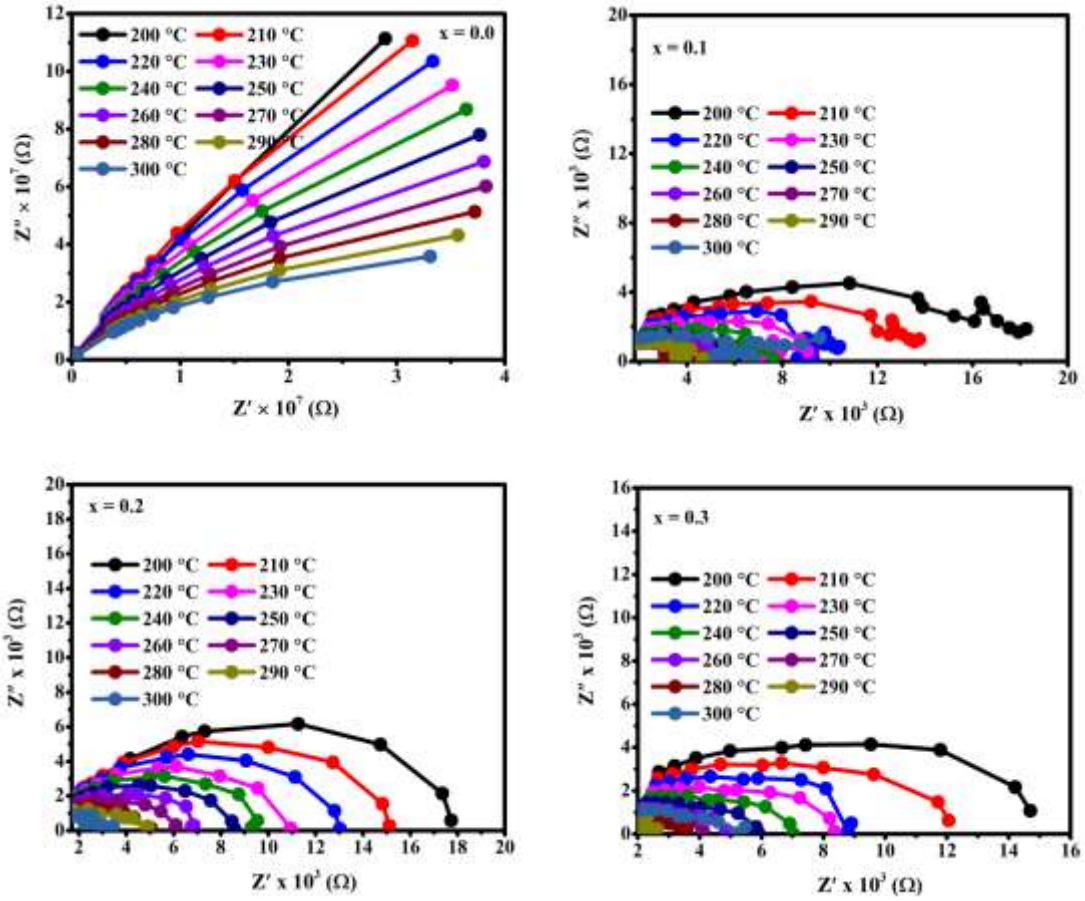

Figure 7. Cole-Cole plots of $Sr_{0.98}$ Zn $_{0.02}$ Ni $_x$Ti$_{(1-x)}$ O_3 (where x = 0.0, 0.1, 0.2 and 0.3) ceramics at different temperatures.

Fig.7 Shows the variation of real part of impedance (Z′) with the imaginary part of impedance (Z″) (Cole – Cole plots) for $Sr_{0.98}$ Zn $_{0.02}$ Ni_x $Ti_{(1-x)}$ O_3 ceramics at different temperatures. From the figure it is clearly observed that the obtained impedance spectra of undoped sample exhibit the straight line (slightly bending), this is because of conduction of bulk and electrode-dielectric interfacial space charge polarization of the material [30]. The figure shows the one semicircle whose center lie below the real axis. According to the Debye's model, a material having single relaxation time gives rise to an ideal semicircle centered on the real axis. Corresponding to the Ni doped $Sr_{0.98}Zn_{0.02}TiO_3$ ceramics a single semicircular arc can be observed at low frequency region. The appearance of single semicircular plot shows depressed semicircle at low frequency, this represents that grain boundary effect and single conductivity process of the ceramic samples [31]. The radius of the semicircular arc can be decreases with increasing the temperature for pure and Ni doped $Sr_{0.98}$ Zn $_{0.02}$ TiO_3 ceramics.

Electrical modulus spectrum analysis

Complex dielectric modulus formulation was solving the relaxation process of the material; in this purpose this method was adopted. The electric modulus gives information about the nature of polycrystalline samples and also describes the electrical relaxation, as a microscopic property of ionic solids. The study of electrical relaxation in this system is carried out by using the dielectric modulus (M*) is given by the reciprocal of the complex permittivity ε* is represented by the following equations.

$$M^* = M' + j\,M'' = \frac{1}{\varepsilon^*}$$

Where M′ and M″ are real and imaginary terms of M*.

$$M^* = M' + j\,M'' = \frac{\varepsilon'}{\varepsilon'^2 + \varepsilon''^2} + j\,\frac{\varepsilon''}{\varepsilon'^2 + \varepsilon''^2}$$

Where ε′ and ε″ is the real and imaginary part of the permittivities.

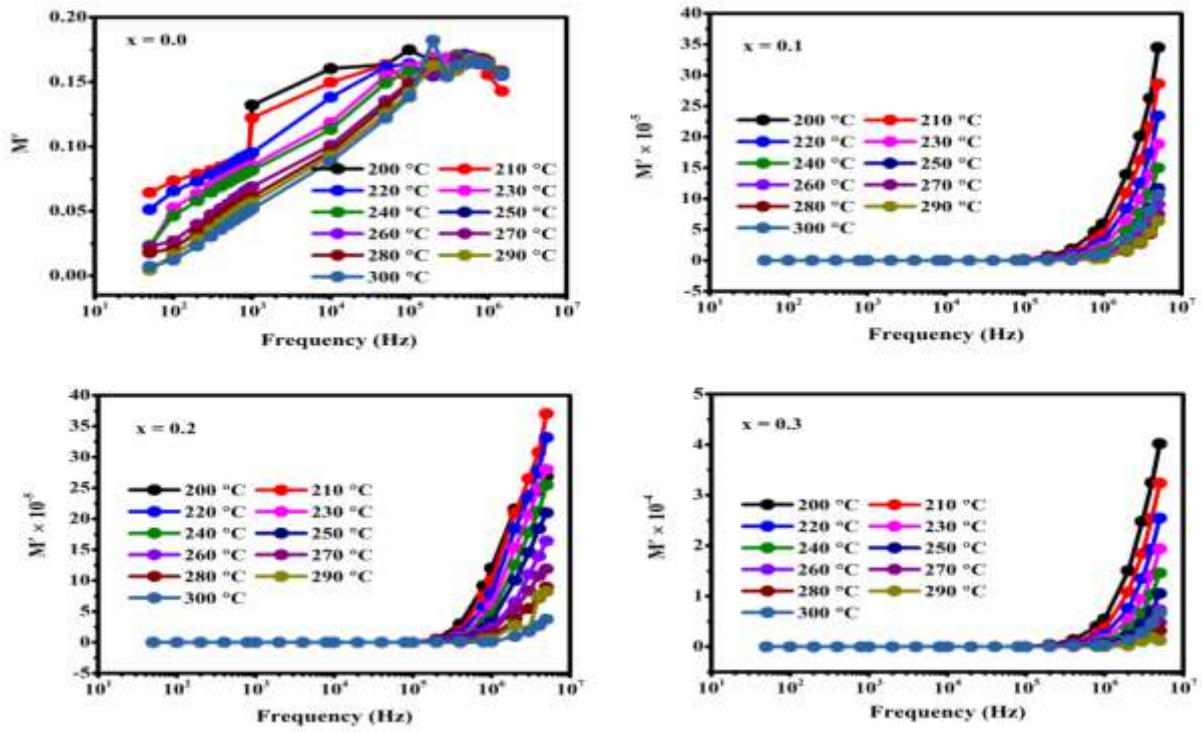

Fig. 8(a) Frequency dependent of real part of the electric modulus spectrum (M′) of $Sr_{0.98}Zn_{0.02}Ni_xTi_{(1-x)}O_3$ (where x = 0.0, 0.1, 0.2 and 0.3) ceramics at different temperatures

Frequency dependent of real part of the electric modulus spectrum of $Sr_{0.98}Zn_{0.02}Ni_xTi_{(1-x)}O_3$ (where x = 0.0, 0.1, 0.2 and 0.3) ceramics at different temperature was displayed in figure. The Ni doped $Sr_{0.98}Zn_{0.02}TiO_3$ it is observed that at low frequency region, the M′ exhibits almost constant values. Because in this region polaron hopping illuminating is occurred. While, at higher frequencies, it observed that an asymmetric peak, it is maximum for all samples. With increasing Ni concentration, the relaxation peaks are diminished and slightly shifted towards at higher frequencies. The asymmetric broadening of the peaks is indicative of the spread of relaxation times with different time constants and the non exponential approach of electrical functions. Hence, this type relaxation should be known as Non-Debye type of relaxation. Moreover, the shift of the asymmetric modulus peaks towards the higher frequency side with increasing temperature indicates correlation between motions of mobile ion charges [32]. This type of the modulus spectrum confirms the existence of hopping mechanism in the electrical conduction of the Ni doped $Sr_{0.98}Zn_{0.02}TiO_3$ studied ceramics.

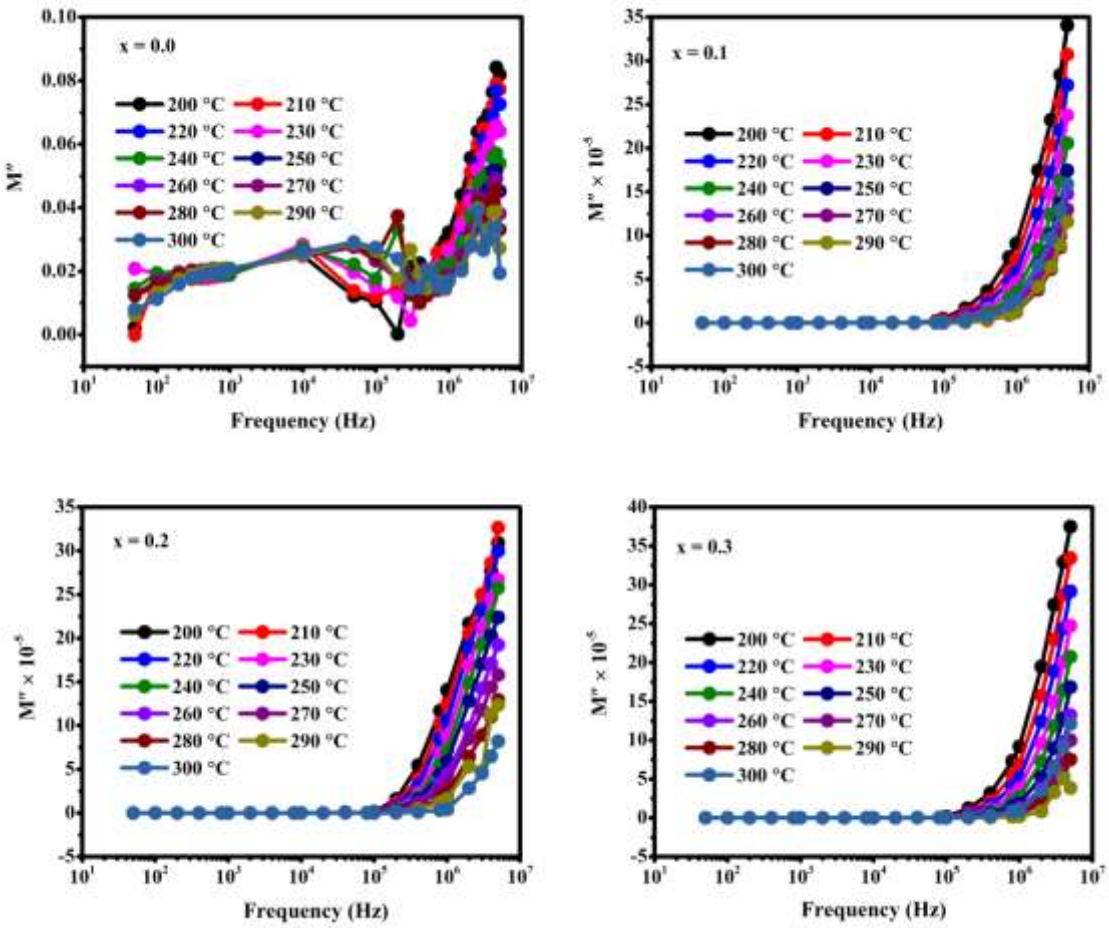

Figure 8(b). Frequency dependent of imaginary part of the electric modulus spectrum (M″) of $Sr_{0.98}$ $Zn_{0.02}$ $Ni_xTi_{(1-x)}$ O_3 (where x = 0.0, 0.1, 0.2 and 0.3) ceramics at different temperatures.

The imaginary part of electric modulus (M″) of Ni doped $Sr_{0.98}Zn_{0.02}TiO_3$ are shown in Fig. 8 (b). The imaginary part of electric modulus spectrum increases at higher frequencies up to 10^6 Hz for all temperatures. Though imaginary part electric modulus is strongly temperature dependent at higher frequencies, because at higher frequencies it shows an asymmetric maximum for all samples. With increasing Ni concentration, the shows that the value of M″ approaches to zero at lower frequencies, because at lower frequencies, it has been associated with a lack of restoring force for the charge stream under the influence of an electric filed [33].

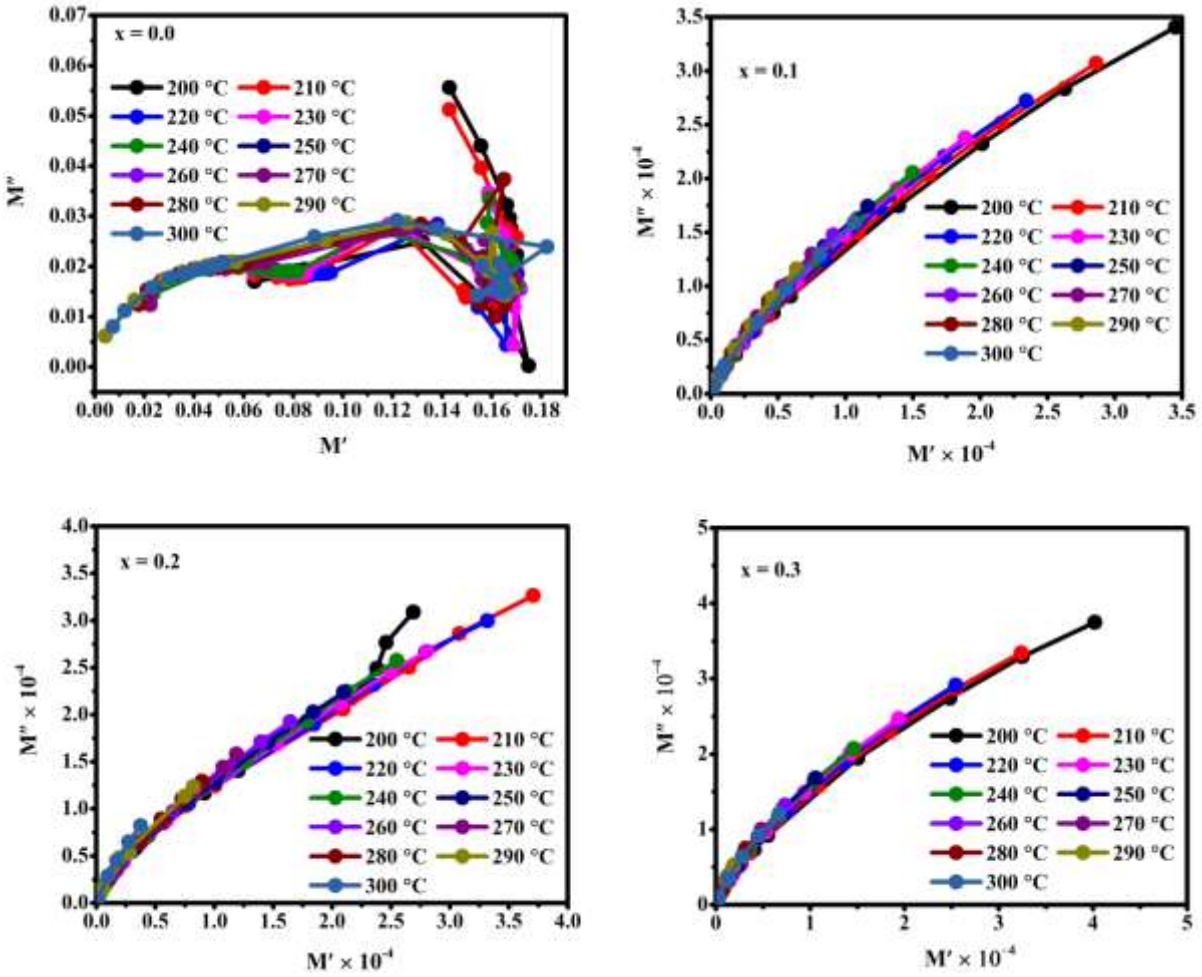

Figure 9. Variation of real and imaginary part of the electric modulus (M′& M″) at different temperatures for (x = 0.0, 0.1, 0.2 and 0.3) ceramics.

The fig 9. Shows the complex modulus plots of M′ verses M″ corresponding various frequencies at different temperatures. The figure observed that in figure x = 0.0 sample the curves show an almost linear type of behavior therefore relaxation process occurred for lower frequencies. Whereas the figures x = 0.1, 0.2 and 0.3 samples the curve changes into a linear shape to semicircle shapes at the beginning of the graph. The coincidence of the beginning of the graph semicircles with the origin of the graph .It is clear that with increasing the concentrations there is no other relaxation process occurred at lower frequencies. The temperature dependence of real and imaginary part of the dielectric modulus spectrum for lower and higher frequencies does not merge into single curves. It conforms at higher temperature the moment of charge carriers is temperature dependent non- Debye type of relaxation behavior [34-35].

Magnetic properties

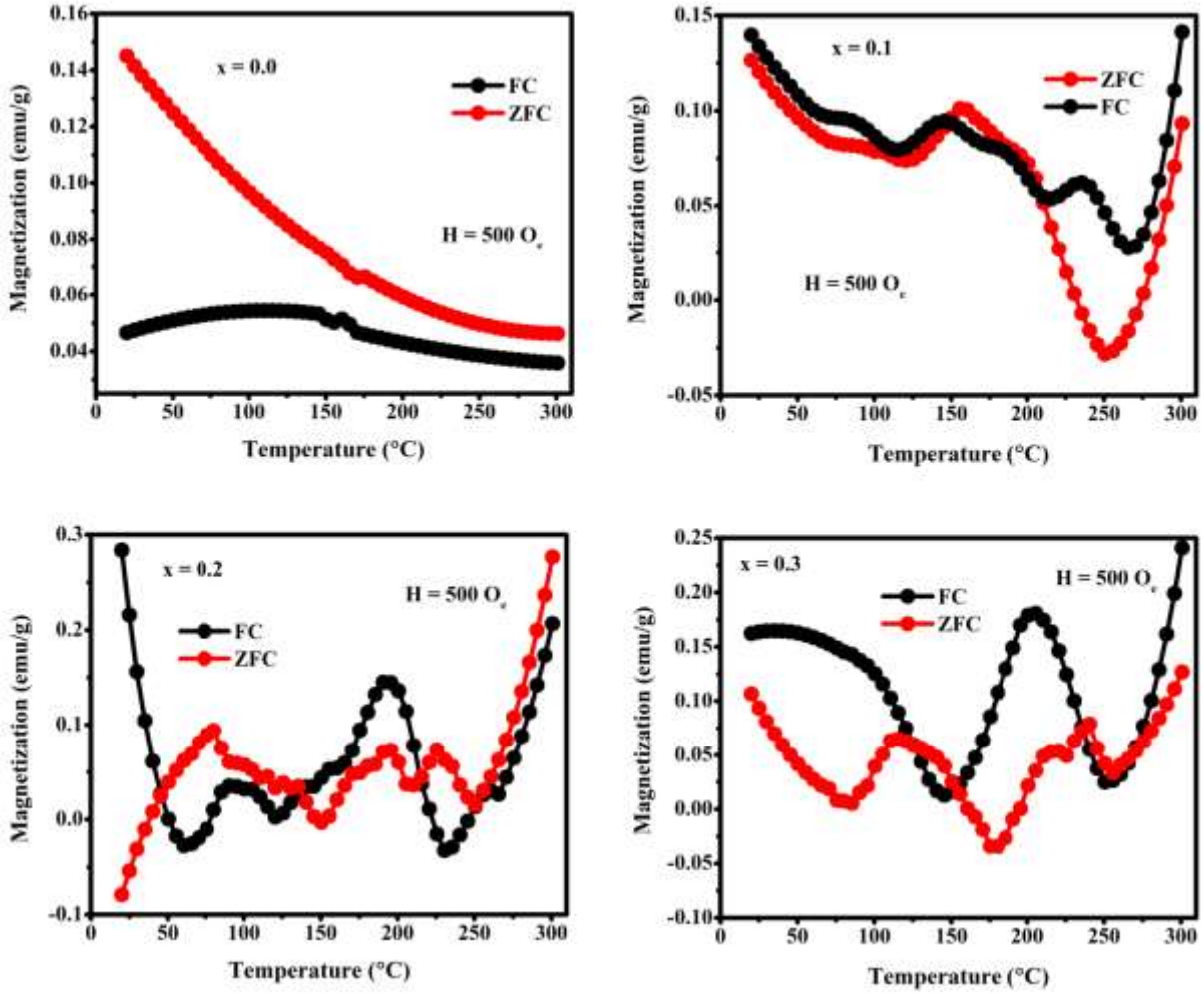

Figure 10 FC-ZFC curves measured at 500 O_e field of $Sr_{0.98}$ Zn $_{0.02}$ Ni_x $Ti_{(1-x)}$ O_3 (where x = 0.0, 0.1, 0.2 and 0.3) ceramics

The temperature dependence of the ZFC and FC magnetization of $Sr_{0.98}$ $Zn_{0.02}$ $Ni_xTi_{(1-x)}$ O_3 (where x = 0.0, 0.1, 0.2 and 0.3) ceramic samples is carried out under an applied field of 500 Oe and low temperature range it is shown in Fig.10. For host material the temperature dependent of ZFC and FC magnetization may be attributed to the appearance of spin-glass like behavior induced by competition between the ferromagnetic and anti ferromagnetic exchange interaction [36]. Hence, an increasing FC magnetization is observed at low temperature, which indicates the presence of short range ferromagnetic ordering [37, 38]. The Ni doped $Sr_{0.98}Zn_{0.02}TiO_3$ ceramics the shape of the M–T curve is concave and the magnetization existence of correlation between the ionic radius of the substituting element and the magnetic properties of the corresponding to the closer ionic radius of Ni^{2+} (0.69Å) to Ti^{4+} (0.61 Å). Hence, weak spin glass or super paramagnetic behavior can be ruled out of my composite. The Ni doped $Sr_{0.98}Zn_{0.02}TiO_3$ ceramics, the FC curves exhibit abrupt increase in their values at certain low temperature, which can be correlated to the weak ferromagnetic nature of the prepared ceramics.

IV. Conclusion

The structural, electrical and magnetic electrical properties of $Sr_{0.98}Zn_{0.02}$ $Ni_xTi_{(1-x)}O_3$ (x = 0.0, 0.1, 0.2 and 0.3) ceramics were successfully prepared by solid state reaction method. The cubic structure of all ceramics have confirmed with X-ray diffraction patterns. Dielectric constant and loss are decrease with an increasing the frequency. Cole-Cole plots shows that the conduction mechanism is due to the grain boundary effect. The dc resistivity is found to decreases with an increase in temperature. The increase in dielectric constant with increasing the temperature is attributed to the conductivity which is directly related to an increase in mobility of localized charge carriers. The imaginary part of the electrical modulus was employed to study the relaxation dynamics of the charge carriers. The electrical relaxation process is occurring to be SZT material was found to be slightly dependent on the Ni concentration and temperature. Particularly at higher temperatures non Debye type of relaxation was clearly observed for all the samples. The temperature dependence of magnetization indicated the weakly ferromagnetic nature and Ni spin ordering ferro/ferromagnetic materials. This present suitable work is applicable to high storage properties of microwave and potential applications.

V. References

[1] Goian V , Kadlec F , Kadlec C , DabrowskiB, Kolesnik S, Chmaissem O, D.Nuzhnyy, Kempa M , Bovtun V , Savinov M , Hejtmanek J, Prokleˇska J , Kamba S. Spectroscopic studies of the ferroelectric and magnetic phasetransitions in multiferroic Sr1−xBaxMnO3. J. Phys. Condens. Matter.2016; 28 :175901-1-7.

[2] Markiewicz E, Bujakiewicz-Koronska R , Nalecz D.M, Kalvane A. Impedancespectroscopy studies of $SrMnO_3$, $BaMnO_3$ and $Ba_{0.5}Sr_{0.5}MnO_3$ ceramicssynthesized by conventional high-temperature method. Phase Trans. 2014; 87: 1060–1072.

[3] Akselrud L, Grin Y.WinCSD: software package for crystallographic calculations (version 4). J. Appl. Crystallogr.2014;47: 803–805.

[4] Bujakiewicz-Koronska R, Nalecz D.M, Markiewicz E, Kalvane A. Electronicproperties of 6H hexagonal SrMnO3. Ferroelectrics. 2015;486: 1–8.

[5] Li L, Liu Y, Qin X, Li D, Zhang J, Song C, Wang L. Enhanced thermoelectric performance of highly dense and fine-grained (Sr1-xGdx)TiO3 ceramics synthesized by sol-gel process and spark plasma sintering. J. Alloys Compd . 2014; 588: 562–567.

[6] Fang L,Dong W, ZhengF, Shen M. Effects of Gd substitution on microstructures and low temperature dielectric relaxation behaviours of $SrTiO_3$ ceramics. J. Appl. Phys. 2012;112: 034114-18.

[7] Tkach A, Vilarinho P.M, Kleemann W, Shvartsman V.V, Borisov P , Bedanta S. Comment on The origin of magnetism in Mn-doped SrTiO3. Adv.Funct. Mater. 2013; 23 : 2229–2230.

[8] Tkach A, Okhay O, Wu A. Vilarinho P.M, Bedanta S. Shvartsman V, Borisov P. Magnetic anomaly and dielectric tunability of (Sr, Mn)TiO3 thin films,Ferroelectrics. 2012; 426: 274–281.

[9] Varignon J, Ghosez P. Improper ferroelectricity and multiferroism in2H-BaMnO3. Phys. Rev. B. 2013;87: 140403(R)-1-4.

[10] Pyatakov A.P, Zvezdin A.K. Magnetoelectric and multiferroic media, Physics (Uspekhi).2012; 55: 557–581.

[11] Yuan X.P, Y. K. Tang Y. K, Sun Y, Xu M. X. Structure and magnetic properties of Y1-xLuxFeO3 ceramics. J. Appl. Phys.2012;111: 053911-16.

[12] Dai ZH, Akishige Y. Electrical properties of multferroic BiFeO3 ceramicssynthesized by spark plasma sintering. J Phys D Appl Phys. 2010; 43: 445403.

[13] Dai ZH, Fujita Y, Akishige Y. Dielectric properties and heating effect of multiferroic BiFeO3 particle suspension. Mater Lett. 2011; 65: 2036.

[14] Lebeugle D, Colson D, Forget A, Viret M: Very large spontaneous electricpolarization in BiFeO3 single crystals at room temperature and its evolution undercycling fields. Appl Phys Lett. 2007; 91: 022907.

[15] Leontsev SO, Eitel RE. Dielectric and Piezoelectric Properties inMn-Modified (1-x)BiFeO3-xBaTiO3 Ceramics. J. Am. Ceram. Soc. 2009; 92:2957-2961.

[16] Yang HB, Zhou CR, Liu XY, Zhou Q, Chen GH, Li WZ and Wang H. Piezoelectric properties and temperature stabilities of Mn and Cu modifiedBiFeO3–BaTiO3 high temperature ceramics. J. Eur. Ceram. Soc. 2013; 33:1177-1183.

[17] Singh SK, Ishiwara H , Maruyama K. Room temperature ferroelectricproperties of Mn-substituted BiFeO3 thin films deposited on Pt electrodes usingchemical solution deposition. Appl. Phys. Lett. 2006; 88: 262908.

[18] Pradhan AK, Zhang K, Hunter D, Dadson JB, Bhattacharya P, Katiyar R, *et.al*. Magnetic and electrical properties of single-phase multiferroic BiFeO3. J Appl Phys. 2005; 97: 093903.

[19] Dang ZM, Shen Y , Nan CW. Dielectric behavior of three-phase percolative Ni-BaTiO3/polyvinylidene fluoride composites. Applied Physics Letters. 2002; 81:4814-4816.

[20] Fischer P, Polomska M, Sosnowska I ,Szymanski M. Temperature-dependence of the crystal and magnetic-structures of BiFeO3. J. Phys. C: Solid State Phys. 1980; 13: 1931-1940.

[21] Claude E, Spaldin N.A. Weak ferromagnetism and magnetoelectric coupling in bismuth ferrite, Phys. Rev. B. 2005; 71: 060401-409.

[22] Jyoshna Rout, Choudhary R. N. P .Structural transformation and multiferroics properties of Ba-Mn co doped BiFeO3. Physics letters A.2016; 380: 288-292.

[23] Arya G. S, Kotnala R. K, Negi N. S. Structural and multiferroic properties Bi1-xInxFeO3 ($0 \leq x \leq .20$) nanoparticles. Journal of applied physics.2013; 113: 044107-109.

[24] Picozzi S, Ederer C. First Principles Studies of Multiferroic Materials, Journal of Physics. Condensed Matter.2009; 21: 303201-303219.

[25] Shivanand Madolappa, Anupama A.V, Jaschin P. W, Varma K.B.R, Sahoo B. Magnetic and ferroelectric characteristics of Gd3+ and Ti4+ co-doped BiFeO3 ceramics Bull. Mater. Sci.2016; 39 (2): 593–601.

[26] Parashar J, Saxena V. K, Jyoti, Bhatnagar D, Sharma K.B. Dielectric behavior of Zn substituted Cu nano-ferrite. J. Magn. Magn. Mater. 2015;394: 105–111.

[27] Gul I.H, Maqsood A, Naeem M, Ashiq M. N.Optical, magnetic and electrical investigation of cobalt ferrite nanoparticles by co-precipitation route. Journal of Alloys and Compounds. 2010; 507: 201-06.

[28] Samita Pattanayak, Choudhary R.N.P, Piyush Das R, Shannigrahi S.R. Effect of Dy substitution on structural, electrical and magnetic properties of multi ferroic BiFeO3 ceramics. Ceramics International.2014;

40: 7983-7991.
[29] Mathur P, Thakur A, Singh M. Low temperature processing of Mn-Zn nanoferrites. Journal of Materials Science.2007; 42:8189-8192.
[30] Thakur A, Thakur P, Hsu JH. Smart magneto dielectric nano-materials for the very high frequency applications. Journal of Alloys and Compounds. 2011; 509: 5315-5319.
[31] Liu T, Xu Y. B, Feng S. S, Zhao J. Y. A facile route to the synthesis of BiFeO3 at low temperature. J. Am. Ceram. Soc. 2011; 94: 3060-3.
[32] Mukherjee A, Hossain S. M, Pal M, Basu S. Effect of Y-doping on optical properties of multiferroics BiFeO3 nanoparticles. Appl. Nanosci. 2012; 2: 305-310.
[33] Zhu Jian, Pavan Kumar N, Min Zhong, Hu Yemin, Venugopal Reddy P.Structural, Magneticand Dielectric Properties of Bi0.9Re0.1FeO3 (Re = La, Sm, Gd and Y). J Supercond Nov Magn. 2015; 28 (9): 2627-2635.
[34] Anjum G, Kumar R, Mollah S, Shukla D.K, Kumar S. Lee C.G. Structural, dielectric, and magnetic properties of La0.8Bi0.2Fe 1−*x*Mn*x*O3 (0.0≥x≥0.4) multiferroics, J. Appl. Phys.2010;107:103916-19.
[35] Bhardwarj S, Paul J, Raina K.K, Thakur N.S, Kumar R. Dielectric modulus and magnetocapacitance behavior of Bi3.7Sm0.3Ti2.7Fe0.3O12 multiferroic. Physica B. 2014; 448: 194-198.
[36] Yang C, Liu C.Z, Wang C.M, Zhang W.G, Jiang J.S. Magnetic and dielectricproperties of alkaline earth Ca2+ and Ba2+ ions co-doped BiFeO3 nanoparticles. Journal ofMagnetism and Magnetic Materials. 2012; 324: 1483-1487.
[37] Kumar P, Kar M. Effect of Structural Transition on Magnetic and Dielectric Properties of La and Mn co-substituted BiFeO3 Ceramics. Mater. Chem. Phys.2014;148: 968-977.
[38] Sharma H.B, Nomita Devi K, Gupta V, Lee J.H, Bobby Singh S. Ac electrical conductivity and magnetic properties of BiFeO3-CoFe2O4 nano composites. Journal of Alloys and Compounds. 2014; 599: 32-39.